JET Volume 6 (2013), p.p. 33 - 50

Issue 1, February 2013

http://www.fe.um.si/en/jet/e-jet.html

THE UNSTEADY STATIC-STALL AERODYNAMIC CHARACTERISTICS OF AN S809 AIRFOIL AT LOW REYNOLDS NUMBERS

AERODINAMIČNE KARAKTERISTIKE NESTACIONARNEGA ZASTOJA NA PROFILU S809 PRI NIZKIH REYNOLDSOVIH ŠTEVILIH

Matej Fike[ℜ], Gorazd Bombek, Matjaž Hriberšek, Aleš Hribernik

Keywords: S809 airfoil, low Reynolds number application, unsteady static-stall

Abstract

An investigation was conducted to study the unsteady static-stall characteristics of an S809 airfoil whose aerodynamic characteristics are representative of a horizontal axis wind-turbine. It is very difficult to experimentally investigate this phenomenon, especially when attempting to study the development of flow-separation when the blades are rotating. The application of wind-tunnel tests or CFD simulation is obviously more appropriate. In order to investigate unsteady static-stall regarding the aerodynamic characteristics of an S809 airfoil, a comparative study was performed to obtain numerical and experimental results for the flow-separation position, airfoil pressure distribution, and velocity profiling that included velocity oscillations. The experimental results were acquired using PIV (Particle Image Velocimetry) and the study was performed at various angles of attack (AOA). No separation was observed at low AOA, but at 9.6° AOA the separation vortex comprised 50% of the airfoil's chord length, whilst a complete stalling of the airfoil occurred at 20° AOA. The observed separation zone was not steady but was found to oscillate around its mean-position at an interval of ± 10% of the chord's length. Neither of the applied turbulence models *k-ε* nor SST used in 2D unsteady

[ℜ] Corresponding author: Matej Fike, Faculty of Mechanical Engineering, University of Maribor, E-mail address: matej.fike@gmail.com

---

simulation predicted this oscillation, although the numerical results agreed fairly well with those experimentally obtained, especially the averaged velocity and vorticity fields around the suction side of the airfoil when using the SST model.

Povzetek

Opravljena je bila raziskava, kjer smo preučevali karakteristike nestacionanega statičnega zastoja na profilu S809, katerega aerodinamične karakteristike so reprezentativne za vetrne turbine z horizontalno osjo. Eksperimentalno je zelo težko preučevati ta pojav, še posebej kadar želimo preučevati odcepljanje toka na rotirajočih lopaticah. Izvedba meritev v zračnem tunelu oziroma simulacij računalniške dinamike tekočin je primernejše. Z namenom raziskovanja nestacionarnega statičnega zastoja glede aerodinamičnih karakteristik S809 profila je bila opravljena primerjalna študija, tako so bili primerjani eksperimentalni in numerični rezultati položaja odcepitve toka, porazdelitve tlaka po profilu in hitrostih profilov vključno z oscilacijami hitrosti. Eksperimentalni rezultati so bili pridobljeni z uporabo PIV (meritev hitrosti z odslikavo delcev) in pri različnih napadnih kotih. Pri nizkih napadnih kotih nismo zaznali odcepitve toka, pri napadnem kotu 9.6° je odcepljen vrtinec zavzemal 50% dolžine tetive profila, pri napadnem kotu 20° zastojni vrtinec obsega ves profil. Opazovana področje odcepitve ni bilo stacionarno ampak smo ugotovili, da oscilira okrog njene srednje pozicije v intervalu ±10% dolžine tetive. Uporabljena turbulentna modela, *k-ε* in SST, v 2D časovno odvisnih simulacijah nista napovedala teh oscilacij, čeprav so se numerični rezultati dokaj dobro ujemali z eksperimentalno pridobljenimi, še posebej polja povprečne hitrosti in polja vrtinčnosti na sesalni strani profila pri uporabi SST turbulentnega modela.

1 INTRODUCTION

Wind-turbines operate within a broad span of wind-speed by starting their operations at 4 m/s and operating up to 24 m/s, this being the usual shut-down wind speed. A turbine's rotational speed is usually constant and the blade-pitch angle fairly rigid. However, if the relative wind-angle increases, this causes an increase in the angle of attack that may lead to flow-separation at the suction sides of the turbine's blades, and eventually to blade-stalling. Although flow-separation should be avoided in aviation unless firm-braking is intended, it is commonly used for wind-turbines. These are designed with a maximum power level that can be reached dozens of times per year. Predicting peak rotor power and post-peak power is important when designing constant-speed and variable-speed stall-regulated rotors. Thus, information about the state of the boundary layer over the suction surface of the airfoil is necessary when designing wind-turbine blades, in order to predict and consider the flow characteristics within the transitional regime. Furthermore, predicting the location of the transition-point is important for those wind turbine applications that operate at low Reynolds numbers. This is because the laminar/turbulent properties of the flow-field have an important influence on the skin-friction and separation that significantly affect both the lift and drag characteristics of the blade. Since the introduction of the boundary-layer concept, scientists and engineers have been facing a constant challenge to minimize its adverse effects, and then use it to their advantage. The present research was conducted to study the unsteady static-stall characteristics of an S809 airfoil, the aerodynamic characteristics of which are representative of a horizontal axis wind-turbine. This was in order to provide a greater understanding of those unsteady flow-separation processes that are effectively used for the stall-regulation of a wind-turbine's rotor.

Low Reynolds number aerodynamics are characteristic for wind turbine applications in which low inflow velocities result in operational regimes with low-to-moderate wing-chord Reynolds numbers (i.e. chord Reynolds numbers ranging from 10,000 to 500,000). Whilst conventional aeronautic design principles usually either neglect the viscosity effect or restrict its influence to a thin region near the airfoil's body at high Reynolds numbers, a predominance of the fluid-viscosity effect for the low Reynolds number applications would result in boundary layers growing rapidly and separating from the surfaces of the airfoils easily, which should never be neglected. The behaviour of the laminar boundary layer on low-Reynolds number airfoils would significantly affect the aerodynamic performance of the airfoils. Since laminar boundary layers are unable to withstand any significant adverse pressure gradient, laminar flow separation is usually found on low-Reynolds-number airfoils. It was suggested by Lissaman, [1], and Mueller, [2], that the separated laminar boundary layers around low-Reynolds-number airfoils would behave more like free shear layers, which are highly unstable and, therefore, the rolling-up of Kelvin-Helmholtz vortex structures and transition to turbulent flows would be readily realised. When the adverse pressure gradient over the airfoil surface becomes large enough, the transition of the separated laminar boundary layer to turbulent flow could be conducted rapidly, and the increased entrainment of the turbulent flow could cause the turbulent flows to reattach to the airfoil's surface as a turbulent boundary layer. This would form what is termed a 'laminar separation bubble'. The reattached turbulent boundary could stay firmly attached to the airfoil surface up to the airfoil trailing edge. As the adverse pressure gradient increased with any increasing angle of attack, a second separation (separation of turbulent boundary layer) could occur. The second separation point would firstly move gradually along the suction surface with an increasing angle of attack, and then, starting at a certain AOA when the adverse pressure gradient had become more severe, it would suddenly (almost instantaneously) jump to the leading edge. This would be because of the sudden bursting of the laminar separation bubble, which would then result in airfoil stall. It has been reported that the position of the separation point in the case of a turbulent boundary layer is not static, [3]. Furthermore, Nishimura and Taniike, [4], showed a correlation between the frequencies of the separation point-position fluctuations and von Karman instability, which subsequently causes fluctuations of the lift and drag coefficient. However, common practice is to use the average values for lift and drag coefficient obtained by steady-state simulations, [5-6], or experimentally measured, [7-8].

The purpose of the presented research was to evaluate the oscillation zone of the turbulent layer's separation point, using a combination of flow visualization by the PIV method and numerical simulation done with CFD code, and to provide a greater understanding of those mechanisms responsible for flow-separation and its influence on lift and drag regarding the S809 airfoil.

2 MATERIALS AND METHODS

2.1 Airfoil section

For this study, an airfoil was chosen whose aerodynamic characteristics were representative of horizontal axis wind-turbine (HAWT) airfoils: the S809. It is a 21% thick, laminar-flow airfoil designed specifically for HAWT applications. A sketch of the airfoil is shown in Figure 1. As

---

reported by Somers, [8], at positive angles of attack below approximately 5°, the flow remains laminar over the forward half of the airfoil. It then undergoes laminar separation followed by a turbulent reattachment. As the angle of attack is increased further, the upper-surface transition point moves forward, and the airfoil begins to experience small amounts of turbulent trailing edge separation. At approximately 9°, the last 5 % to 10% of the upper surface is separated. The upper-surface transition point has moved forward to approximately the leading edge. As the angle of attack increases to 15°, the separated region moves forward to about the mid-chord. With further increases in the angle of attack, the separation moves rapidly forward to the vicinity of the leading edge, so that at about 20°, most of the upper surface is stalled. According to this, the presented investigations were focused on four different angles of attack: 5.1°, 9.6°, 15.1°, and 20.0°, respectively.

2.2 Wind tunnel

The experiments were performed within a small wind-tunnel (cross-section 200 × 200 mm). The maximum air velocity in the tunnel was 36.3 m/s, and the turbulence intensity, measured by hot wire anemometry, was 1.5%. The size of the airfoil was designed according to the tunnel's dimensions and the desired pressure taps for pressure measurement. The airfoil was produced using rapid prototyping, and the chord's length (c) was selected as 100 mm, resulting in Reynolds number Re = 2×10^5 at maximum air-speed. A transparent extension was added to the wind-tunnel to enable PIV measurements. This extension and the airfoil fixture enabled a setting of the airfoil's angle of attack. The airfoil and the locations of the pressure measurement points are presented in Fig 1.

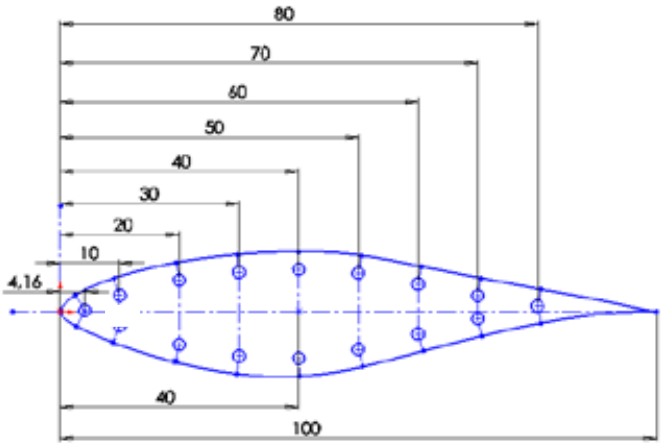

Figure 1: *Geometry of the airfoil and the pressure-tap's locations*

Sixteen positions for pressure measurements were applied, and 50 mm-long pneumatic tubes were used for connecting with the sensors. The sinusoidal response of the plastic tubing and sensors was, therefore, satisfactory for frequencies up to 300 Hz, since the gain factor was less

than 1.05, [9]. Therefore, the frequency response of the system was satisfactory because the phenomena investigated, in particular the Von Karman vortex shedding, had a characteristic frequency below 300 Hz. GMSD 2.5 MR and GMSD 25 MR pressure sensors were used, with different measurement uncertainties of 0.5 Pa and 5 Pa, respectively. Pressure signals within durations of 10 seconds were acquired with 1 kHz sampling frequency.

2.3 PIV system

The Dantec PIV (Particle Image Velocimetry) system was used to capture the flow-field around the airfoil (Fig. 2). The camera and laser were placed on a lightweight traverse system originally used for LDA measurements. A measurement plane was placed in the middle of the airfoil to reduce the influence of the wall. A two-cavity Nd: YAG laser was used, operating at high power with 50 mJ pulse energy. The frequency of bursts was 4 Hz. A fog-generator was used for seeding in order to produce seeding particles with average diameters of 1 μm. The laser was placed downstream at approx. 1 m from the airfoil. A CCD camera with 1280 × 1024 pixels resolution was used, and the area covered was approx. 120 × 100 mm. The time-interval between the laser pulses was 20 μs, and 32 × 32 pixel-size interrogation areas were used for velocity calculation. Cross-correlation and adaptive correlation were used, both with 25% overlap.

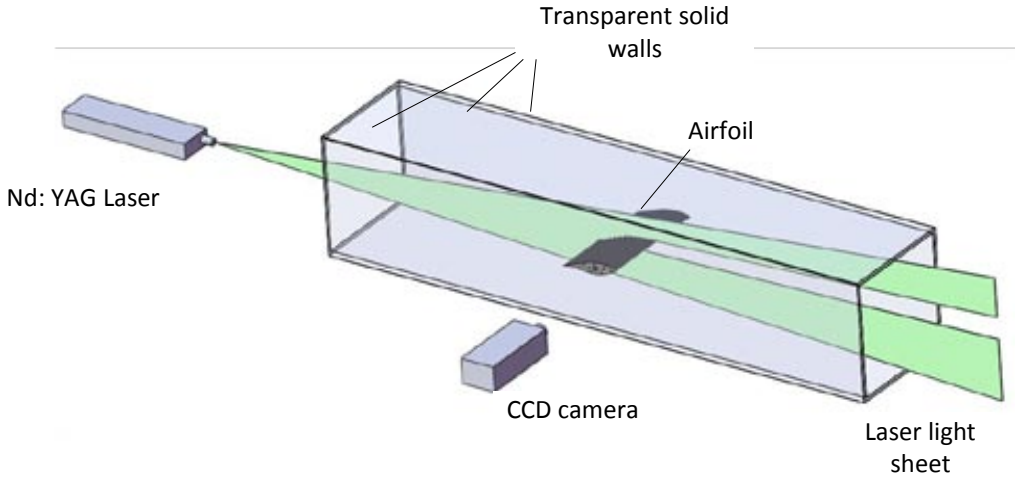

Figure 2: *The PIV measurement system*

Several parameters have to be considered when estimating the uncertainties of PIV velocity measurements, [10]. Systematic errors occur due to uncertainties in determining the geometrical parameters and the fabrication tolerances of the camera's devices and lenses. Non-systematic errors are mainly due to the uncertainty when determining the average particle displacement within the interrogated region. These depend on the size of the interrogated region, the time separation between the laser pulses, the magnification of the recording, the

---

out-of-plane velocity component, the turbulence, the length-scale of the flow etc. As the flow within the test-section was quasi-two-dimensional, the out-of-plane component of the vectors only caused negligible errors. Lehr and Boelcs, [11], showed that for these conditions the standard measurement uncertainty for the mean velocity field is less than 0.04 u_∞, and in the regions of strong velocity gradients it is smaller than 0.05 u_∞.

2.4 Numerical simulations

2D numerical simulations were performed for airfoil flow analysis. The simulations were conducted at the same geometry and angles of attack as used during the experiment. Steady-state and transient simulations were made, and the turbulence model selections were limited to k-ε and SST (Shear Stress Transport) models. The Ansys 12.0 CFX code, [12], and the 2nd-order high-resolution scheme were used. An RMS residual below 10^{-6} or a stationary value of lift and drag coefficient were used as the convergence criterion. Computational meshes were created using ICEM-CFD. Precise analysis of the laminar transition boundary layer was possible only if the spatial resolution of the grid near the wall satisfied the condition $y^+<1$, whilst the value $y^+>30$ was required in the case of the k-ε model. Since a scalable wall-function was used, the same computation mesh satisfying the condition $y^+<1$ was used when applying the k-ε model. A block-structured mesh type C with 119,000 nodes was used for 2D simulations. The simulation area was extended to two chord-lengths in front of the airfoil and to five chord lengths behind it. The tunnel's actual height (two chord lengths) was used. Fig. 3 shows an excerpt of the computational mesh close to the airfoil. No slip-boundary condition was used on the walls of the wind-tunnel. A constant velocity with a measured turbulence level of 1.5% and a static pressure boundary condition were applied at both the inlet and outlet, respectively. The GCI (Grid Convergence Index method) was used, [13], in order to calculate numerical uncertainty. The numerical uncertainty of the separation point location was 0.5%.

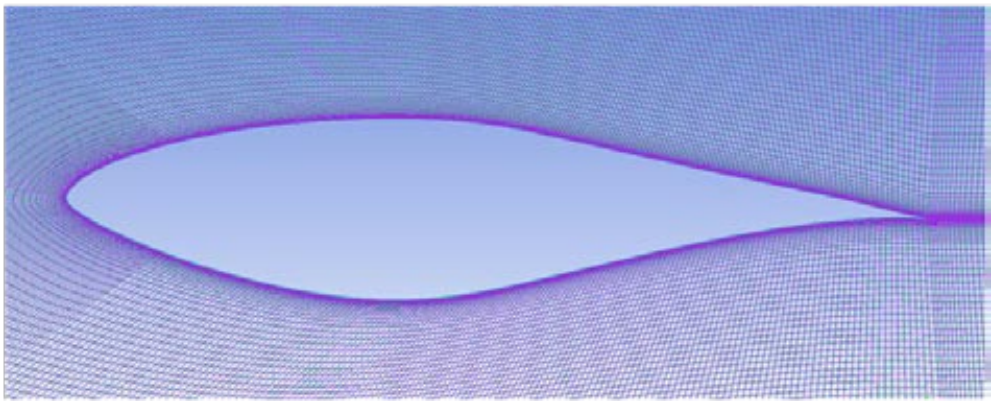

Figure 3: *Detail of the computational mesh close to the airfoil*

---

3 RESULTS

As mentioned, the presented investigations were focused on the study of turbulent layer separation from the suction side of the airfoil. This separation may happen at moderate AOA after the reattached turbulent boundary layer separates again from the airfoil surface. The turbulent boundary layer separation is greatly influenced by von Karman instability, which causes the separation point to oscillate. Simpson et al., [3], proposed a set of quantitative definitions on the detachment state near the wall using definitions based on the fraction of time the flow moves downstream. Four characteristic points were defined: incipient detachment (ID) occurring with an instantaneous backflow 1% of the time, transitory detachment (TD) occurring with an instantaneous backflow 50% of the time, and detachment (D) occurring where the time-averaged wall shear stress was equal to zero. Available data indicated that the TD and D points were at the same location, [3]. Finally, the characteristic point Dcp determines a critical position downstream of which the flow is detached at any time. In the following, the experimental results based on PIV images and pressure measurements are presented, followed by the numerical results and a comparison.

3.1 PIV images analysis

The PIV system operated at frequencies of up to 4 Hz, and disallowed direct time-dependent analysis of the flow-field around the airfoil. Therefore, at least 60 consecutive images were acquired and their corresponding velocity fields established. The averaged velocity fields around the airfoil measured at four different AOA are presented in Fig. 4. No turbulent boundary layer separation occurred at 5° AOA. At 9.6° and 15.1° AOA, backflow vortex in the backward half of the airfoil indicated turbulent layer separation and a partially-stalled airfoil, whilst the burst of laminar separation bubble near the leading edge appeared at 20° AOA, and most of the suction surface was stalled, which agreed with the findings of Somers, [8].

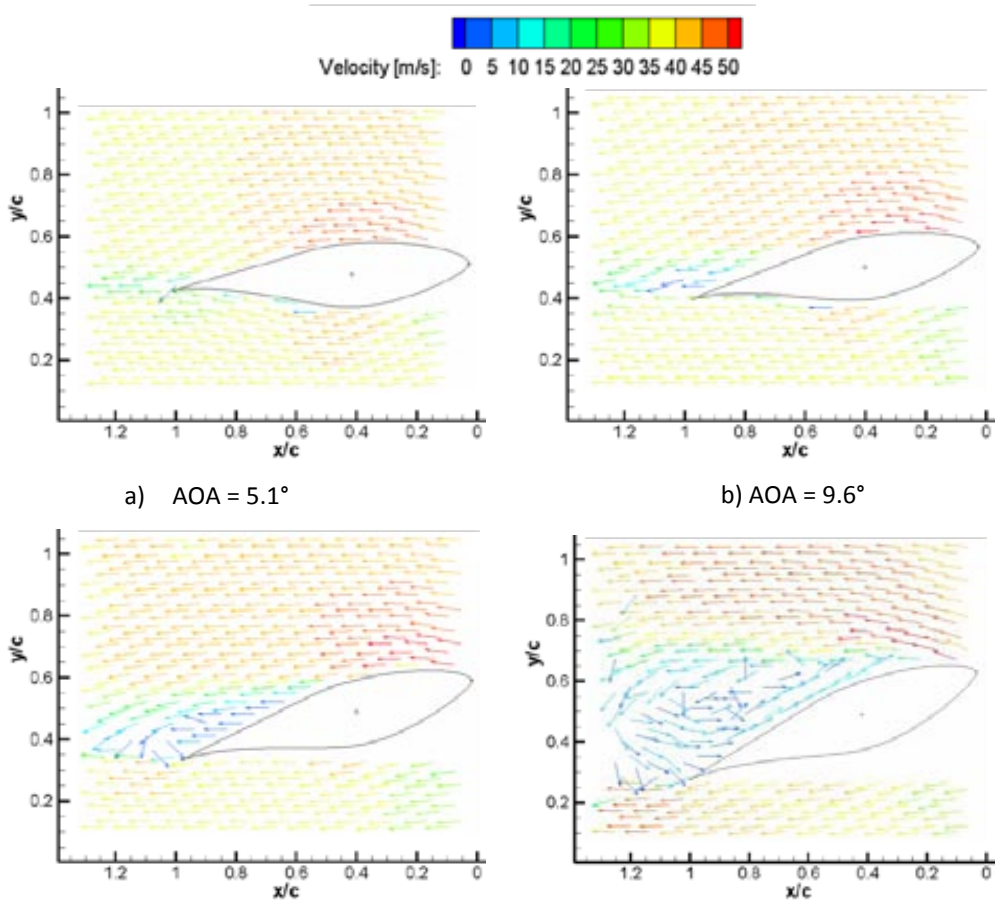

Figure 4: *Velocity fields around the airfoil acquired by PIV, Re = 2 × 10^5*

The fluctuating nature of the flow-separation was evident from successive PIV images. Two characteristic images that proved the oscillation of the flow-separation point at 15.1° AOA are presented in Fig. 5. Whilst in the right image flow separation occurred at *x/c* = 0.4, it shifted towards the trailing-edge of the airfoil by *x/c* = 0.6 in the left image.

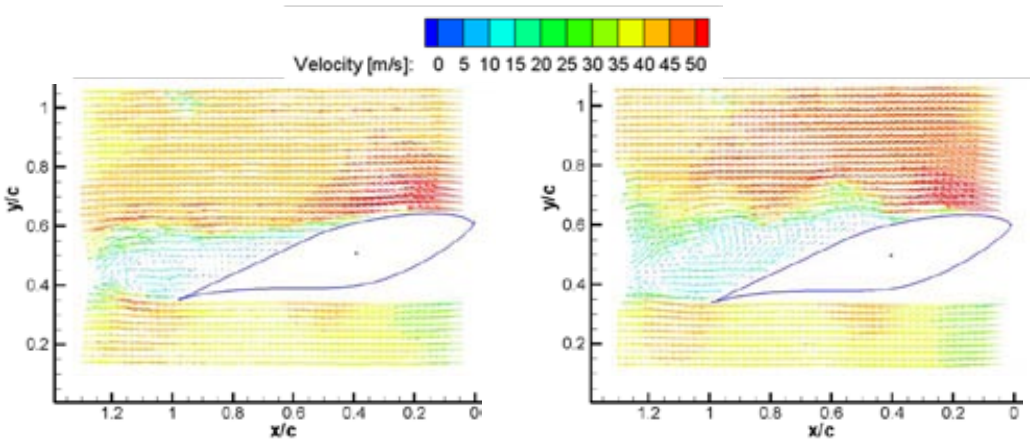

a) Separation point at x/c = 0.6 *b) Separation point at x/c = 0.4*

Figure 5: *Two characteristic PIV images proving the oscillation of the flow separation point AOA = 15.1°, Re = 2 × 10^5*

By careful analysis of a series of PIV images taken at the same AOA over a longer period of time, the separation zone could be further studied in order to predict not only both extreme points ID and Dcp, but also to estimate the percentage of back-flow at any point within the separation zone. A program was developed in LabVIEW to use the PIV results and extract all the values for each vector (velocity components, position and status). It was possible to analyse the data and calculate the medium value and standard deviation for the velocity and its direction (angle). It was also possible to count those cases in which the angle differed from the chord angle by more than a certain value. If the value was set at 90°, the result represented backflow occurrence. This value could be divided by the number of images, resulting in a backflow occurrence ratio. The results can be presented as intensity graphs, as shown in Fig. 6.

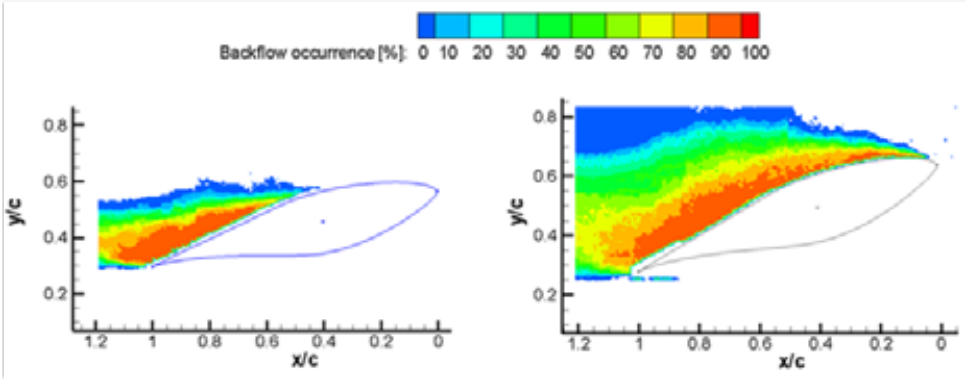

a) AOA=15.1° b) AOA=20.0 °

Figure 6: *Intensity graph of the backflow occurrence ratio; Re = 2 × 10^5*

As can be seen from Fig. 6a (AOA = 15.1°), the alternations between the attached and separated flow (ID point) occurred at *x/c* = 0.4 (area with 0 to 10% of backflow). At *x/c* = 0.47 the flow was reversed 50% of the time; therefore, this point corresponded to the transitory detachment (TD) point, and at *x/c* = 0.62 the flow was detached at any time and corresponded to the Dcp point. The separation zone stretched between *x/c* = 0.4 and *x/c* = 0.62 at 15.1° AOA, but at 20° AOA (Fig. 6b) it comprised only a short region near the leading edge, actually representing the laminar separation bubble (LSB) which had moved forward and burst due to severe adverse pressure gradient.

Similarly, the series of images at both the other two AOAs were analysed, and the results are presented in Table 1. The separation point oscillation-zone moved towards the trailing-edge when AOA decreased. In the case of 20° AOA, permanent flow-separation occurred at *x/c* = 0.11 with the bursting of the LSB, which was spread between 0.02 < *x/c* < 0.11 and the airfoil suction side was totally stalled. Partial-stall was observed at 15.1° AOA and 9.6° AOA. The turbulent boundary layer was first reattached and then the second separation took place with the oscillation zones between 0.40 < *x/c* < 0.62 for AOA = 15.1° and 0.48 < *x/c* < 0.66 for AOA = 9.6°, respectively. No separation of turbulent boundary layer was observed in the case of 5.1° AOA.

Table 1: *Comparison between the experimentally obtained positions (x/c) of the characteristic points (ID, TD, Dcp) of the flow separation zone and the predicted results*

	Angle of attack (°)							
	5.1	9.6			15.1			20
		ID	TD	Dcp	ID	TD	Dcp	LSB burst
PIV images analysis	NS*	0.48	0.52	0.66	0.40	0.47	0.62	0.02–0.11
Pressure signal analysis	NS	0.5		0.6	0.3		0.6	0.0–0.2
Simulation, *k-ε* turb. model	NS	NS			0.63			0.37**
Simulation, SST turb. model	0.92	0.53			0.42			0.01**

**NS – no separation occurred*

***LSB burst was not predicted by the k-ε and SST turbulence models; therefore, the data corresponds predicted flow separation position*

3.2 Pressure tap signal analysis

Eight pressure taps on each side of the airfoil (Fig. 1) were used for instantaneous pressure signal measurements. When averaged, these signals could be used to obtain pressure profile around the airfoil. Pressure is usually presented in the form of a pressure coefficient:

$$C_p = \frac{p - p_\infty}{\frac{1}{2}\rho u_\infty^2} \tag{3.1}$$

where p_∞ is the free-stream static pressure and u_∞ the free-stream velocity far upstream from the airfoil. In order to validate the obtained pressure profiles, a comparison was made with the results obtained by Sommers et al., [8]. Fig. 7 shows a comparison between pressure coefficient profiles at AOA = 9.6°. The agreement was good and ensured that the presented measurements are correct.

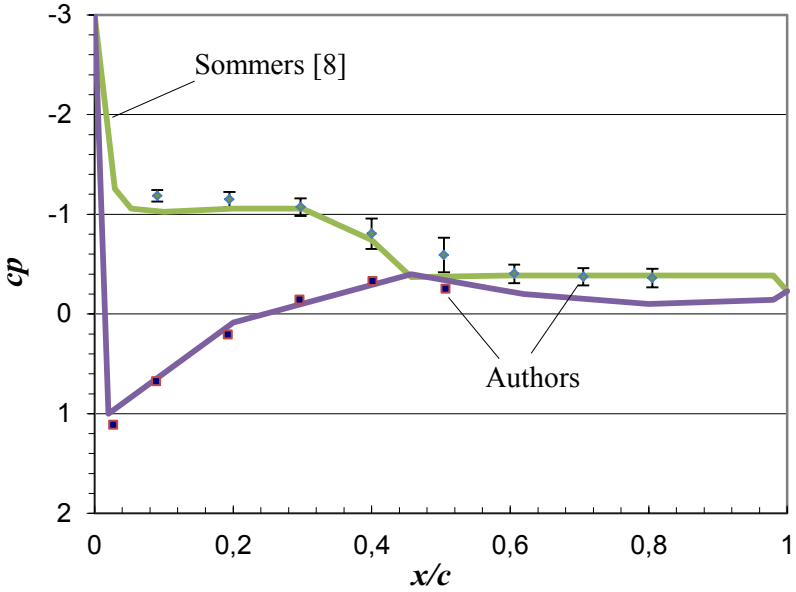

Figure 7: *Pressure coefficient profile for AOA = 9.6°*

Besides obtaining the tap position's averaged pressure, the acquired pressure signals may also be used to calculate the signal standard deviation, which represents the measure of pressure fluctuation intensity at a particular tap position. Along with the averaged pressure coefficient, its standard deviation for the airfoil suction side is also presented in Fig. 7. As can be seen, it varied alongside the airfoil with a maximum value at approximately *x/c* = 0.5. According to Sicot et al. [14], the oscillation zone of the flow-separation point can be obtained using standard deviation of the signals from the pressure taps along the suction-side of the airfoil. The curves connecting these values for AOA = 5.1°, where (according to PIV images) no stall was presented and AOA = 9.6°, where the airfoil was partially stalled, were compared and are shown in Fig. 8. The difference was quite evident. The curve for AOA = 5.1° has no local extremes, whilst these are clearly evident in the curve for AOA = 9.6° which had two characteristic points. The first one corresponds to the incipient detachment point (ID). This ID point represents the position of the separation point where the alterations occurred between the attached and separated flows. Therefore, the pressure fluctuations at the ID point were the greatest, thus coinciding with the local maximum value for normalized standard deviation. Upstream of ID, the flow is attached at any moment. The characteristic point Dcp downstream from which the flow is detached at any

---

time corresponds, according to Sicot et al. [14], to the local minimum of standard deviation. The interval between the ID and Dcp points locates the oscillation zone of the separation point. The error made using this method comes from the discontinuous distribution of the pressure taps. The resolution was quite low in the presented case, since only 8 pressure taps were applied on the airfoil suction's surface. Similarly, the series of pressure signals at all other AOA were analysed, and the results are presented in Table 1 for comparison with the results obtained from PIV images, and the numerical predictions. The presented pressure signal based method adopted from Sicot et al. [14] predicts only both extreme points (ID and Dcp) within the separation point-oscillation zone, and gives no quantitative insight into it unlike the PIV method. However, it is very robust and may be applied for the first approximation of the position and length of the separation point oscillation zone. In the presented case (Table 1), the predicted separation point oscillating zone agreed fairly well with the results of the PIV based method. The agreement was very good especially at 9.6° AOA. The results at 15.1° AOA were less accurate, whilst the total airfoil suction surface stall at 20° AOA was again correctly predicted.

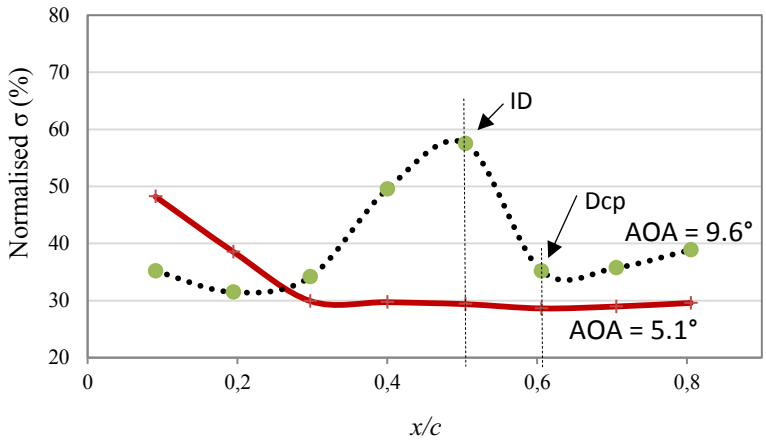

Figure 8: *Variations in the normalised standard deviations of pressure signals from successive pressure taps on the suction side of the airfoil for AOA = 5.1° and AOA = 9.6°, Re = 2 × 10^5*

3.3 Numerical simulation

The last part of the presented study was devoted to numerical simulations. The idea was to obtain better insight into the separation area, in order to understand any possible mechanisms responsible for turbulent layer separation, and oscillation of the separation point. However, the presented work was limited to the application of 2D U-RANS simulation, due to limited computational resources otherwise necessary to run 3D LES or DNS. According to, [15], the 3D U-RANS simulation results appear to be close to a spanwise repetition of the 2D field. The reason for this is due to the role of the 3D spanwise random perturbations that affect the vortex shedding within the real flow. These effects are not described by U-RANS computation, which is intrinsically deterministic, [16]. The 3D U-RANS simulations were therefore omitted.

Two-dimensional steady state simulations were performed during the first step in order to optimise the computational mesh and to obtain the initial conditions for unsteady simulations. Two turbulence models, *k-ε* and SST model, were applied. The *k-ε* turbulence model is the most-widely used turbulence model and enables acceptable predictions when separation is absent (small angles of attack), [17]. However, this model does not consider the transport of shear stress under conditions where separation is caused by an adverse pressure gradient, thus resulting in an overestimation of eddy viscosity and, consequently, estimating both the separation point and separation area inaccurately, resulting in a stalled delay phenomenon. Menter et al., [18], developed the SST turbulence model by improving some weaknesses of the *k-ε* model. Compared to the *k-ε* model, SST provides more accurate predictions of the separation point's position, and the separation area caused by an adverse pressure gradient.

In order to check for the accuracy of simulations, a comparison was made between the measured and computed lift and drag coefficients. The results are presented in Fig. 9. At instances of lower AOA of up to 9.6°, the lift and drag coefficients were well predicted, whilst both the *k-ε* and SST models, respectively, overestimated the lift coefficient and underestimated the drag coefficient at higher AOA, where the airfoil was partially or fully stalled. As was discovered during the experiments performed by the PIV, as well as by instantaneous pressure measurements, the separation point oscillated significantly, especially when the airfoil was partially stalled. It was, therefore, suspected that the poor accuracies of the simulations at high AOA were caused by the steady-state numerical computation. Thus, transient 2D simulations using a SST turbulence model were then carried out; however, the results did not differ significantly from those obtained using steady-state simulations, except for when the AOA = 20°. An oscillating Von Karman vortex street, formed behind the airfoil after the simulation was started, slowly died away, and the final result was a totally-static flow field around the airfoil with no oscillations presented, and the separation point remained static. It is assumed that the reason for this is the overly large turbulent viscosity of RANS turbulent models, which are, therefore, highly dissipative and are unlikely to be triggered into unsteady mode unless the flow instabilities are large, [19]. The latter was the case at AOA = 20°. At this very high AOA, the reattachment of a turbulent boundary layer failed, and total stall took place with a fully turbulent wake behind the leading edge. The predictions were thus in good qualitative agreement with the experimental results (Fig. 4d); however, the damping of oscillations was still too high. The predicted Strouhal number, which should have been around St = 0.2 [14], was less than 0.1 and the mean predicted lift and drag coefficients remained overestimated.

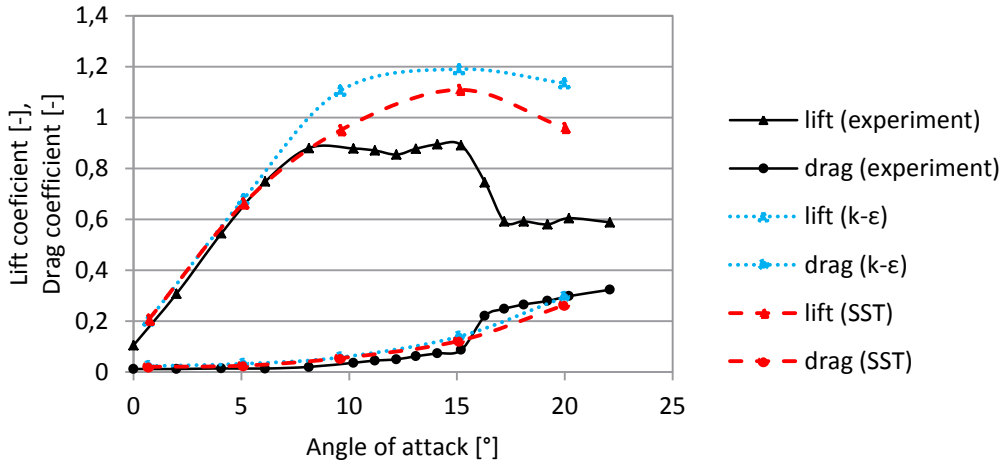

Figure 9: *Comparison between experimentally and numerically obtained lift and drag coefficients; Re = 2 × 10^5*

Since the 2D numerical simulations of partially stalled airfoils at 9.6° and 15.1° AOA could not show any oscillation of the flow-separation point location and predicted only the permanently-detached flow vortex (Fig. 11), it was impossible to determine all the characteristic separation points proposed by Simpson et al., [3], except for the Dcp point location. However, when considering what the steady-state result of an oscillating phenomenon is, this point can be regarded as point TD, where the flow is separated 50% of the time.

Table 1 presents both the experimentally and numerically-predicted flow-separation points. There were substantial differences between the numerical results from different turbulence models. Both the experimental results and the *k-ε* turbulence model's prediction showed no separation on the suction side of the airfoil, whilst the SST turbulence model predicted a small vortex on the trailing edge at 5.1° AOA. The difference increased with any increase in the angle of attack. At 9.6° AOA, no vortex was predicted by the *k-ε* model, although some reduction in velocity was observed, whilst the SST model predicted the flow-separation at x/c = 0.53. At 15.1° AOA, a difference in vortex location was also observed. The flow-separation point predicted by the *k-ε* model was located at x/c = 0.63, whilst the SST model predicted this location at x/c = 0.42. In the case of 20° AOA, a simulation using the *k-ε* model predicted separation at x/c = 0.37, whilst the SST model predicted no reattachment of the turbulent layer, and the flow separated completely at x/c = 0.01 (Fig. 10). Fig. 10 shows a comparison between flow separations predicted using the SST model at 15.1° AOA and 20.0° AOA. At AOA = 15.1° (Fig. 10a), a small vortex was formed at the suction side of the airfoil approximately 0.04 *c* from the leading edge. The flow separated due to sudden directional change when hitting the airfoil and then reattached to the airfoil surface using the high turbulent energy of the main flow. It remained attached to the airfoil until another separation occurred at x/c = 0.42 due to the adverse pressure gradient. No leading edge vortex was formed at AOA = 20.0° (Fig. 10b). The main flow turbulent energy was insufficient to reattach the flow again, and a total stalling of the airfoil occurred. It has to be pointed out that the vortex predicted at AOA = 15.1° should not be

confused with the laminar separation bubble, since the simulation was fully turbulent and could not predict it.

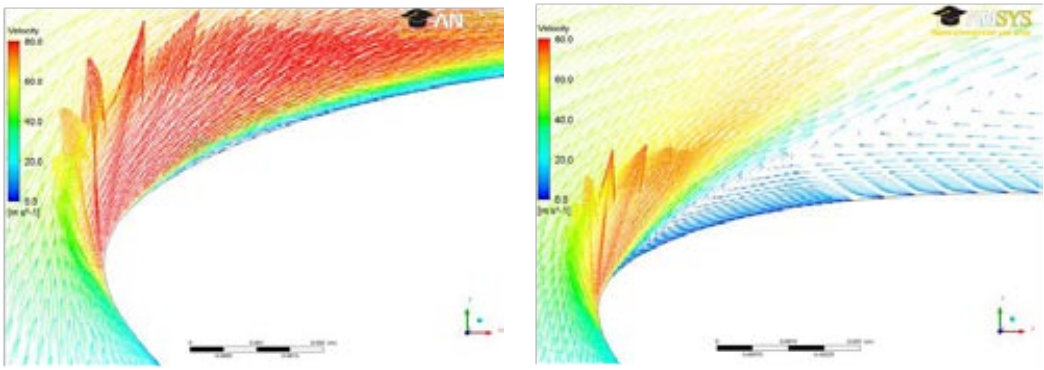

a) AOA = 15.1° b) AOA = 20.0°

Figure 10: *Flow separation predicted using the SST model; Re = 2 × 10^5*

Although both models, *k-ε* and SST, failed to predict the time-dependent behaviour of the turbulent layer separation phenomenon that was established by the experiment at 9.6° and 15.1° AOA, their results could be used as a time-averaged state and (as will be seen later) do agree fairly well with the averaged experimental results, especially for the results of the SST model. Fig. 11 shows a comparison between the predicted and experimentally-obtained time-averaged flow-fields. The latter were obtained by averaging all the instantaneous PIV images corresponding to a particular AOA. A much better agreement with the experimental data was achieved by the SST model, which more accurately predicted the separation vortex at the suction side of the airfoil, in comparison with the *k-ε* model. In contrast, both turbulence models predicted similar velocity fields within the leading edge area and along the whole pressure side of the airfoil. No comparison between velocities within the boundary layer was possible, due to the intense laser light reflection near the airfoil's surface, which prevented any velocity measurements within this area.

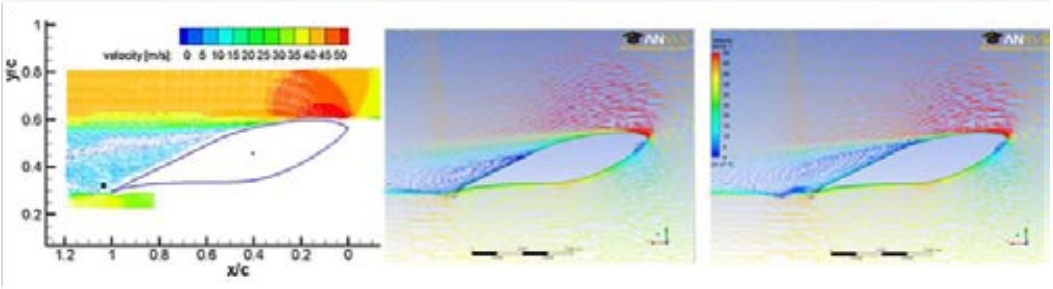

a) PIV b) *k-ε* model c) SST model

Figure 11: *Comparison between the velocity fields of the numerical and averaged experimental results AOA = 15.1°; Re = 2 × 10^5*

The experimentally-obtained average vorticity field (Fig. 12a) showed the formation of two shear layers: one from the leading edge and one from the trailing edge. The formation length was greater from the leading edge (l_2) than from the trailing edge (l_1). A sudden growth of the average shear layer, combined with a roll-up of the shear layer, was observed downstream of the airfoil. Similar results were obtained by Sicot et al., [14], and Yang et al., [20], when they both investigated the flow-field around an isolated airfoil at moderate Re numbers. The numerical simulation using the *k-ε* model predicted no flow separation at 9.6° AOA (see Table 1); thus, no shear-layer was observed from the leading edge (Fig. 12b). The SST model predicted both shear layers quite accurately, although their structures were more compact, and both were longer.

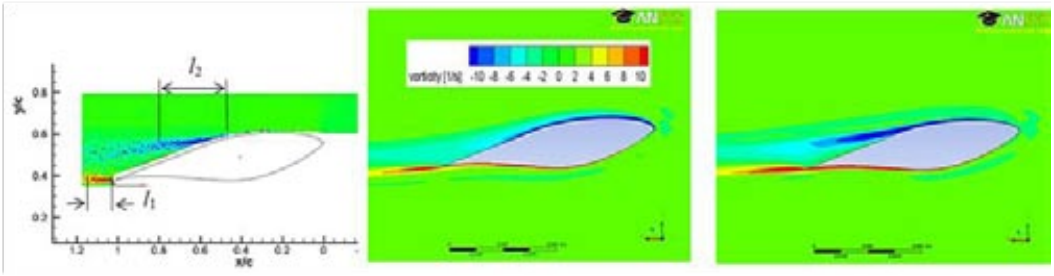

a) PIV b) *k-ε* model c) SST model

Figure 12: *Comparison between the vorticity fields of the numerical (2D) and averaged experimental results AOA = 9.6°; Re = 2 × 10^5*

4 CONCLUSIONS

The unsteady static stall aerodynamic characteristics of an S809 airfoil at low Re numbers were analysed, using both experimental and numerical approaches. Several angles of attack were studied. The PIV system was used to acquire a series of captures in order to obtain instantaneous velocity fields around the suction-side of the airfoil. At low AOA, no flow separation was observed, whilst the already moderate AOA caused the reattached turbulent boundary layer to separate again near the trailing edge of the airfoil, which was therefore partially stalled. With any increasing of AOA, the separation point moved increasingly towards the leading edge until reattachment failed and the airfoil became totally stalled. Instantaneous PIV captures revealed the oscillating nature of the separation point. A simple numerical procedure was applied to obtain a characteristic interval for the separation point's positional oscillation spreading between the permanent separation point and the starting separation point. The experimental part also included pressure profile measurements along the airfoil, and time-dependent measurements of the pressure-oscillation within the specified points around it. The data were analysed and specific points were located for defining the permanent separation points and starting separation points. The results from both experimental methods agree fairly well.

An attempt was also made to simulate the separation point's positional oscillations with CFD simulations. A transient 2D approach using *k-ε* and an SST turbulence model was used; however, both models failed to predict the separation point's positional oscillations. The possible reason for this is due to the role of the 3D spanwise random perturbations that affect the vortex shedding in the real flow, [21]. Although the simulations were unsuccessful in

predicting the oscillatory nature of the separation point, their results showed reliable agreement with the averaged velocity and vorticity fields around the suction side of the airfoil obtained by PIV. The SST model showed better agreement with the experimental data. Although the 3D effects were omitted, the predicted shear layer formations at the leading and trailing-edges agreed well with the averaged experimental results.

References

[1] **Lissaman, P.B.S.**, Low-Reynolds-number airfoils, *Annual Review of Fluid Mechanics*, Vol. 15, 1983, pp. 223–239.

[2] **Mueller, T.J.** (ed.), Fixed and flapping wing aerodynamics for micro air vehicle applications, *Progress in Astronautics and Aeronautics*, ISBN 1-56347-517-0, AIAA, 2001.

[3] **Simpson, R.L., Chew, Y.T., Shivaprasad, B.G.**, The structure of a separating turbulent boundary layer: part I, mean flow and Reynolds stresses; part II, higher order turbulence results. *The Journal of Fluid Mechanics* 113, 1981, pp. 23–73.

[4] **Nishimura, H., Taniike, Y.**, Aerodynamics characteristics of fluctuating forces on a circular cylinder. *Journal of Wind Engineering and Industrial Aerodynamics*, 89, 2001, pp. 713–723.

[5] **Kim, B.S.**; *A Study on the Optimum Blade Design and the Aerodynamic Performance Analysis for the Horizontal Axis Wind Turbines,* Ph.D. Thesis, Korea Maritime University, 2005.

[6] **Wolfe, W.P., Ochs., S.S.**, *CFD calculation of S809 aerodynamic characteristics.* AIAA- 97-0973, 1997.

[7] **Devinant, P., Laverne, T., Hureau, J.**, Experimental study of wind-turbine airfoil aerodynamics in high turbulence, *Journal of Wind Engineering and Industrial Aerodynamics*, 90, 2002, pp. 689–707

[8] **Sommers, D.M.**, *Design and Experimental Results for the S809 Airfoil*, NREL/SR-440-6918, 1997.

[9] **Chapin, W. G.**, *Dynamic-pressure measurement using an electronically scanned pressure module*, NACA TM-84650, 1983.

[10] **Raffel, M., Willert, C., Kompenhans, J.**, *Particle Image Velocimetry: A Practical Guide,* ISBN 3-540–63683-8, Springer-Verlag., 1998.

[11] **Lehr, A., Bölcs, A.**, *Application of a particle image velocimetry system to the investigation of unsteady transonic flows in turbomachinery,* 9th International Symposium on Unsteady Aerodynamics, Aeroacoustics and Aeroelasticity of Turbomachines, Lyon, 2000, pp. 4–8.

[12] Ansys. CFX-SolverTheory Guide, Release 12.1, (2009).

[13] **Celik, I. B., Ghia, U., Roache, P. J.**, Procedure for estimation and reporting of uncertainty due to discretization in CFD applications. *Journal of Fluids Engineering*, Vol. 130, No. 7., 2008.

[14] **Sicot, C., Aubrun, S., Loyer, S., Devinan, P.**, Unsteady characteristics of the static stall of an airfoil subjected to freestream turbulence level up to 16%. *Experiments in Fluids*, 41, 2006, pp. 641–648.

[15] **Jacob, M.C., Boudet, J., Casalino, D.**, A rod-airfoil experiment as benchmark for broadband noise modeling, *Theoret. Comput. Fluid Dynamics*, 19, 2005, pp. 171–196.

[16] **Casalino, D., Jacob, M.C.**: Prediction of aerodynamic sound from circular rods via spanwise statistical modeling. *Journal of Sound and Vibrations*, 262, 2003, pp. 815–844.

---

[17] **Jošt, D., Lipej, A.**, *Numerical prediction of the vortex rope in the draft tube.* Proceedings of the 3rd IAHR International Meeting of the Workgroup on Cavitation and Dynamic Problems in Hydraulic Machinery and Systems, Brno: University of Technology, Brno, 2009, pp. 14–16.

[18] **Menter, F.R.**, Two-equation eddy-viscosity turbulence models for engineering applications. *AIAA Journal*, 32(8), 1994, pp. 1598–1605.

[19] **Davidson, L.**, *Evaluation of the SST-SAS model: channel flow, asymmetric diffuser and axi-symmetric hill,* European Conference on Computational Fluid Dynamics ECCPMAS CFD 2006, Delft, the Netherlands, 2006.

[20] **Yang, Z., Haan, F. L., Hui, H., Ma, H.**, *An Experimental Investigation on the Flow Separation on a Low-Reynolds-Number Airfoil,* 45th AIAA Aerospace Sciences Meeting and Exhibition, Reno Nevada, USA, AIAA-2007-0275, 2007.

[21] **Lammers, P., Jovanović, J., Durst, F.**, *Numerical experiments on wall turbulence at low Reynolds numbers,* Thermal Science; Vol. 10, No 2, 2006, pp. 33–62